



# The composition and structure of volcanic rifted continental margins in the North Atlantic: Further insight from shear waves

Jennifer D. Eccles <sup>a,\*</sup>, Robert S. White <sup>a</sup>, Philip A.F. Christie <sup>b</sup>

<sup>a</sup> Bullard Laboratories, Department of Earth Sciences, University of Cambridge, Madingley Rise, Cambridge CB3 0EZ, UK

<sup>b</sup> Schlumberger Cambridge Research, High Cross, Madingley Road, Cambridge CB3 0EL, UK

## ARTICLE INFO

### Article history:

Received 14 January 2009

Received in revised form 17 December 2009

Accepted 7 February 2010

Available online 12 February 2010

### Keywords:

Volcanic rifted continental margin

North Atlantic Igneous Province

Ocean Bottom Seismometers

Seismic tomography

## ABSTRACT

Imaging challenges caused by highly attenuative flood basalt sequences have resulted in the understanding of volcanic rifted continental margins lagging behind that of non-volcanic rifted and convergent margins. Massive volcanism occurred during break-up at 70% of the passive margins bordering the Atlantic Ocean, the causes and dynamics of which are still debated. This paper shows results from traveltome tomography of compressional and converted shear wave arrivals recorded on 170 four-component ocean bottom seismometers along two North Atlantic continental margin profiles. This traveltome tomography was performed using two different approaches. The first, a flexible layer-based parameterisation, enables the quality control of traveltome picks and investigation of the crustal structure. The second, with a regularised grid-based parameterisation, requires correction of converted shear wave traveltimes to effective symmetric raypaths and allows exploration of the model space via Monte Carlo analyses.

The velocity models indicate high lower-crustal velocities and sharp transitions in both velocity and  $V_p/V_s$  ratios across the continent-ocean transition. The velocities are consistent with established mixing trends between felsic continental crust and high magnesium mafic rock on both margins. Interpretation of the high quality seismic reflection profile on the Faroe margin confirms that this mixing is through crustal intrusion. Converted shear wave data also provide constraints on the sub-basalt lithology on the Faroe margin, which is interpreted as a pre-break-up Mesozoic to Paleocene sedimentary system intruded by sills.

© 2010 Elsevier B.V. All rights reserved.

## 1. Introduction

Volcanic rifted continental margins represent an important subgroup of large igneous provinces (LIPs). Fig. 1 shows the global distribution of these LIPs and other 'hotspot' related volcanism (Coffin and Eldholm, 1994). LIPs cause important additions of igneous material to the crust and potentially important fluxes of heat and volatiles from the mantle (Self et al., 2008). Theories to explain the diverse geological, geochemical and geophysical observations made at LIPs are still controversial with the relative role of mantle temperature, active or passive upwelling and mantle composition actively debated (e.g., Sheth, 1999; Holbrook et al., 2001; Foulger et al., 2005; White et al., 2008).

At volcanic rifted margins, continental break-up was accompanied by the extrusion and intrusion of large volumes of dominantly basaltic magma (Menzies et al., 2002). Such margins are characterised by seaward dipping reflector (SDR) sequences. These represent flood basalt sequences that flowed landward away from the transiently uplifted rift but underwent dip reversal as further stretching, loading

and subsidence occurred (Mutter et al., 1982; Planke and Eldholm, 1994; Spitzer et al., 2008).

The early Tertiary North Atlantic Igneous Province (NAIP; Fig. 1) contains >1 million km<sup>3</sup> of extruded lava (Eldholm and Grue, 1994). Flood basalts flowed up to 150 km outward from the subaerial axial rift (Spitzer et al., 2008) and are more than 7 km thick on the Faroe Islands (Passey and Bell, 2007). Localised extension in the North Atlantic region had been initiated in the Devonian (Dean et al., 1999), with further rifting in the Permo-Triassic as the super-continent Pangea broke-up (Glennie, 1995). More significant regional extension occurred in the Cretaceous with reactivation of pre-existing Caledonide thrusts (Dean et al., 1999). Thus significant pre-breakup depocentres existed between northwest Europe and Greenland which were later buried beneath the Tertiary flood basalt flows. The locus of rifting had shifted westward due to strengthening of the mantle beneath the stretched crust by conductive cooling (Newman and White, 1997) and proceeded to full continental break-up in the Paleocene (Smallwood and White, 2002).

While in many regions seismic reflection imaging of the crust provides structural and morphological control, at volcanic rifted margins the blanketing basalt flows reduce the efficiency of this technique. Although mafic crystalline rocks have low intrinsic attenuation (e.g., Nakamura and Koyama, 1982), the cyclic nature of the basalt flow sequences, with rough

\* Corresponding author. Institute of Earth Science and Engineering, University of Auckland, Auckland 1142, New Zealand. Fax: +64 4223 360779.

E-mail addresses: [j.eccles@auckland.ac.nz](mailto:j.eccles@auckland.ac.nz) (J.D. Eccles), [\(R.S. White\)](mailto:rsw1@cam.ac.uk), [pafc1@slb.com](mailto:pafc1@slb.com) (P.A.F. Christie).

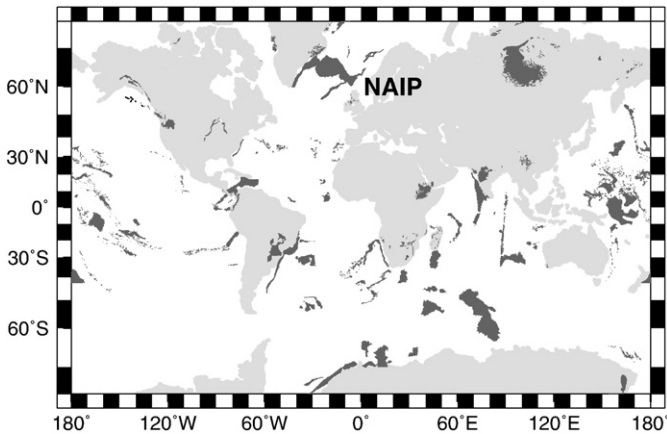


**Fig. 1.** Global distribution of large igneous provinces (shaded in black), including continental flood basalts, volcanic rifted continental margins and oceanic plateaus, and hotspot related volcanism. Compilation by Coffin and Eldholm (1994). The North Atlantic Igneous Province (NAIP), the subject of this study, is labelled. Volcanic rifted continental margins are thought to represent up to 70% of the Atlantic Ocean's passive margins (Clift, 1999; Planke et al., 1999).

surfaces, high velocity massive flow cores and low velocity fractured or vesicular flow margins and interbedded sediments, leads to high effective attenuation. This is due to scattering, complex multiples and mode conversion (Pujol and Smithson, 1991; White et al., 2003; Maresh et al., 2006). Seismic wave induced fluid flow within pores and micro-cracks has also been suggested as a contributor to the high attenuation of basalt sequences (Shaw et al., 2008). Attenuation can be described by the Quality Factor ( $Q$ ): Scheirer and Hobbs, 1990), with high attenuation indicated by the low values (15–40) of effective  $Q_p$  measured for basalt sequences (Rutledge and Winkler, 1989; Maresh and White, 2005; Christie et al., 2006; Maresh et al., 2006; Shaw et al., 2008). The frequency-dependent nature of the attenuation is illustrated by Fig. 2. The basalt flow sequences significantly attenuate the high frequencies, with the

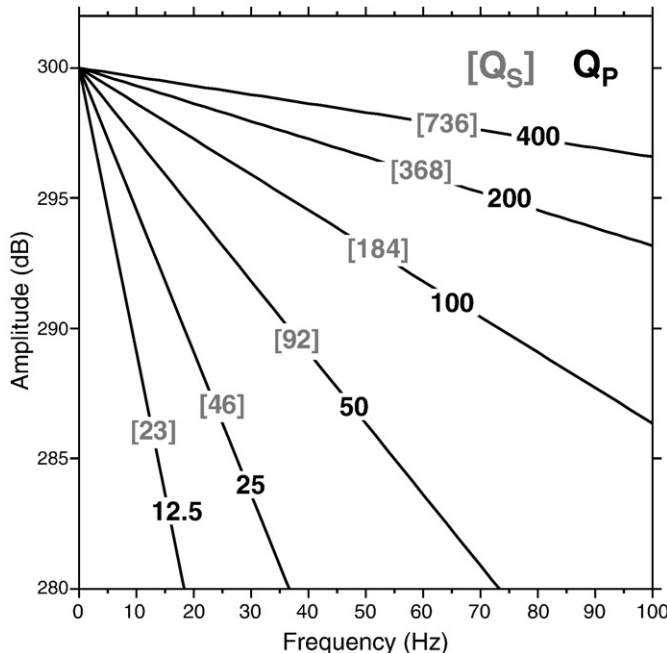


**Fig. 2.** Frequency-dependent effect of variable  $Q_p$  (black) and  $Q_s$  (grey) on amplitude calculated (Maresh et al., 2006) by two-way transmission through a 1 km thick basalt layer with a P-wave velocity of 4 km/s and  $V_p/V_s$  ratio of 1.84 (Christensen, 1996). Geometrical spreading is not considered. The seismic source for this simple model is assumed to have an amplitude of 300 dB (estimated from the direct arrival) across all frequencies.

amplitude of frequencies above 15 Hz typically below the level of noise. Shear (S-) waves have slower velocities through the basalt and  $Q_s$  is estimated to be  $4/9 Q_p$  (Lay and Wallace, 1995), leading to the even greater attenuation of the high frequency energy observed for converted S-waves (Fig. 2).

The integrated Seismic Imaging and Modelling of Margins (iSIMM) project specifically tailored data acquisition to the sub-basalt problem. Seismic data were collected across two margins in the North Atlantic (Fig. 3): the Faroes margin (Profile 1) in the region of most voluminous magmatism and, further to the south, the Hatton Bank margin (Profiles 2 and 3) close to a previous classic transect (Fowler et al., 1989; Spence et al., 1989). Large (6360 in.<sup>3</sup>) airgun arrays were towed at ~18 m depth to produce a low frequency source. There is a trade-off between increased low frequency energy generated by interference of the primary with the sea-surface ghost, which lowers the first notch in the frequency domain as the source is towed deeper (Lunnion et al., 2003), and increased high frequency energy with increased ambient water pressure (i.e., increased tow depth) following the Rayleigh–Willis relation (Christie et al., 2004). The peak frequency of the iSIMM source was 9–11 Hz (Lunnion et al., 2003).

Long offset acquisition enabled more effective velocity analyses to be made and sub-basalt reflectors to be identified. The deployment of 170 ocean bottom seismometers (OBSs) allowed the wide-angle elastic wavefield to be directly recorded at the seabed. Arrivals are observable to source–receiver distances of up to 180 km. Wide-angle compressional (P-) wave arrivals have previously allowed joint refraction and reflection traveltime tomography of these profiles to be carried out (Parkin and White, 2008; White et al., 2008; White and Smith, 2009; Roberts et al., 2009). The value of long offsets has also been demonstrated by the multichannel seismic (MCS) reflection data collected by towed streamers; WesternGeco collected coincident MCS data across the Faroes margin (Profile 1) using a 12 km single-sensor streamer (WesternGeco, 2002), which resolved structure never

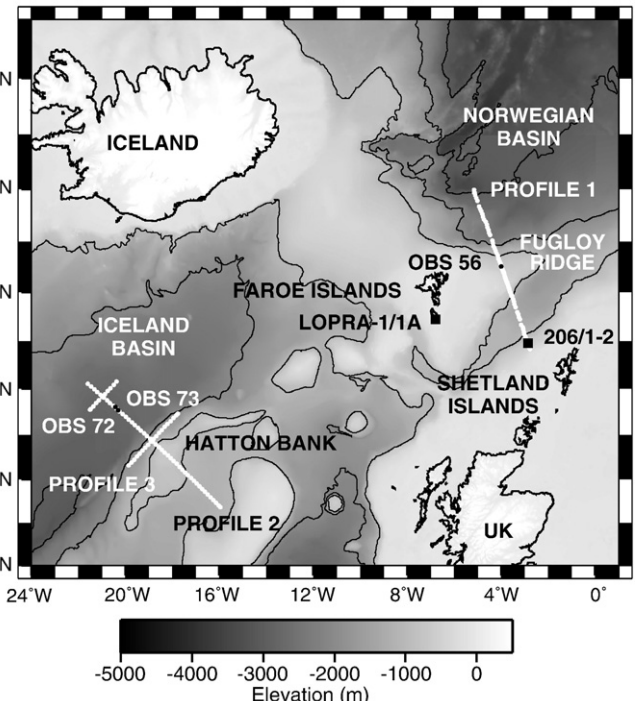


**Fig. 3.** Location map of iSIMM profiles in the North Atlantic region. Bathymetric contour interval is 500 m. OBS deployed across the Faroes and Hatton Bank margins are shown by white circles, example instruments OBS72 and OBS73 from Profile 2 and OBS56 from Profile 1 are highlighted in black. Important boreholes on the Faroe Islands (Lopra-1/1A; Christie et al. (2006)) and Faroe–Shetland Trough (206/1-2) are shown by black squares.

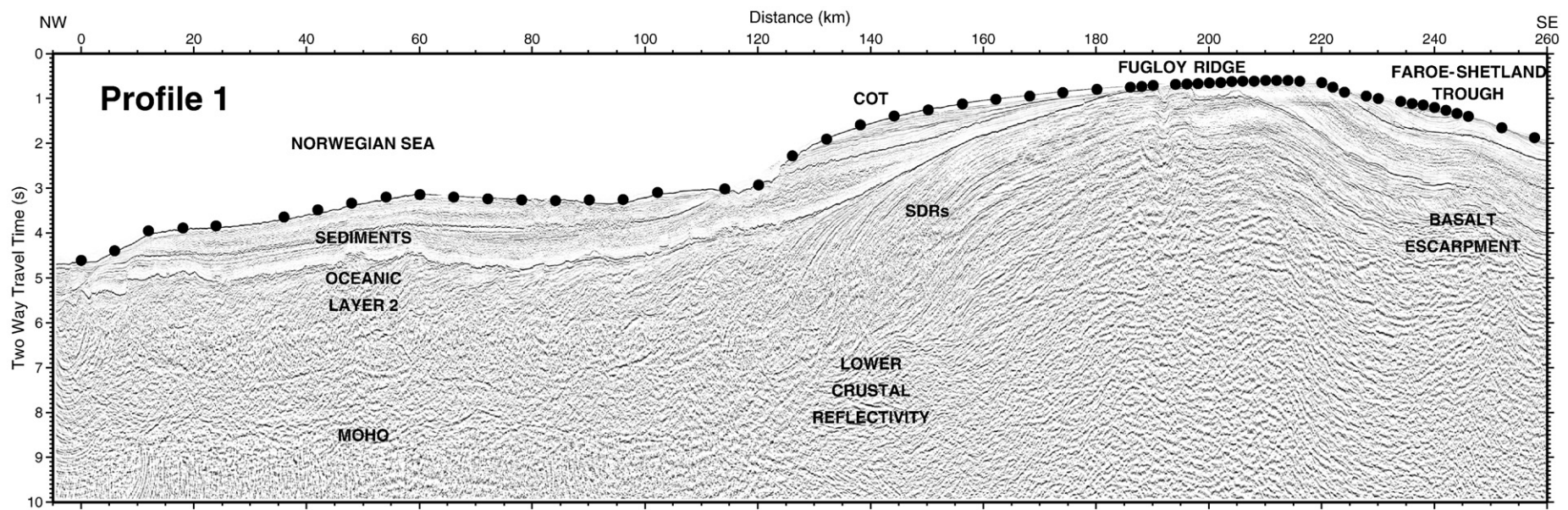


**Fig. 4.** Faroes Profile 1 MCS data collected with a 12 km, single-sensor streamer. Courtesy of WesternGeco. OBS positions are shown by black circles. Features of interest are labelled including characteristic SDR sequences and lower-crustal reflectivity at the continent–ocean transition (COT).

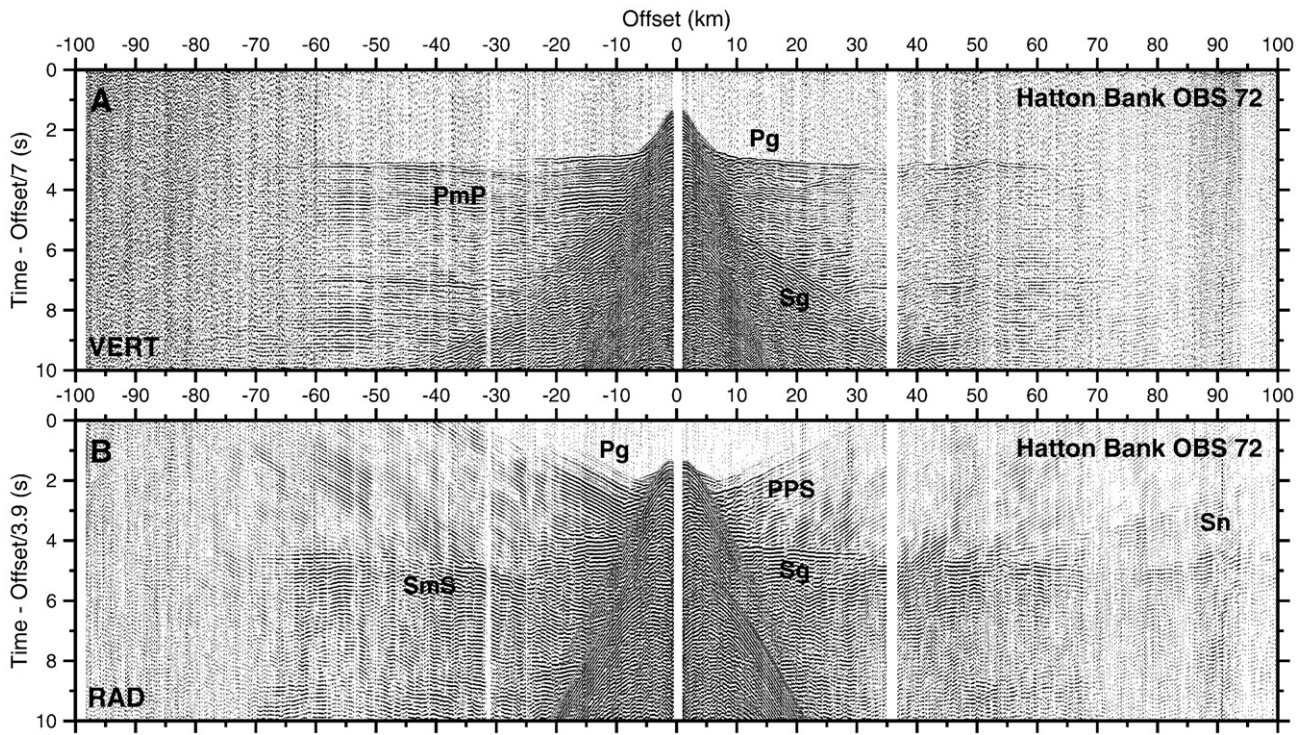


**Fig. 5.** OBS data example from Profile 2 with arrival phases discussed in the text labelled. A. Vertical geophone component of OBS 72 from the Icelandic Basin (location shown in Fig. 3). The receiver gather is displayed with a reduction velocity of 7 km/s. B. Rotated radial geophone component of OBS 72 displayed with a reduction velocity of 3.9 km/s.

before imaged (Fig. 4) and have significantly higher quality than those collected using a similar low frequency source, but a 3 km streamer, across the Hatton Bank margin (Profile 2) (Eccles et al., 2009a).

While MCS images provide structural control and the P-wave velocity models give some constraint on crustal composition, the interpretations

remain somewhat ambiguous. S-wave velocities, giving Poisson's Ratio or  $V_p/V_s$ , allow further constraint to be placed on the physical properties and hence the composition of the crust. The S-wave arrivals used in this study were recorded directly by the four-component OBSs deployed on the seafloor, but conversion from P- to S-waves at an elastic interface was

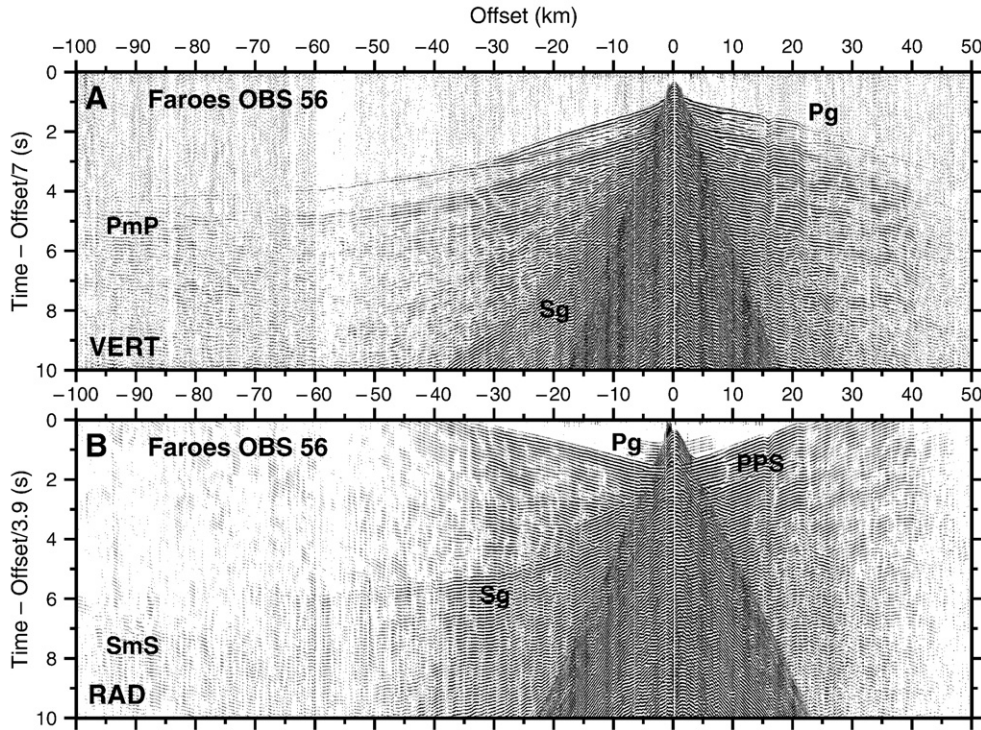


**Fig. 6.** OBS data example from Profile 1 (Faroes) with arrival phases discussed in the text labelled. A. Vertical component of OBS 56 from the Fugloy Ridge (Fig. 3). Reduction velocity is 7 km/s. B. Rotated radial geophone component of OBS 56. Reduction velocity is 3.9 km/s. Note that the earliest arriving Pg refraction is barely visible on this radial component and the strong phase with a P-wave moveout is actually the converted PPS phase delayed by its S-wave path through the post-volcanic sediments.

required to produce these phases from the acoustic wave emitted by the airgun source in the water. Due to their fundamentally different mode of propagation, returning P- and S-waves refracted to near-vertical by low velocity seafloor sediments, have a natural separation and were recorded dominantly on the vertical and horizontal geophone components respectively.

This paper complements the methodology discussed by Eccles et al. (2009a) and presents a more in-depth discussion of the S-wave behaviour and consequent interpretations of volcanic rifted continental margins.

## 2. Arrival phases and conversion interfaces

OBS data examples recorded on Profile 2 OBS 72, situated on oceanic crust of the Iceland Basin, and on Profile 1 OBS 56, from the Fugloy Ridge, are shown in Figs. 5 and 6. These are displayed with reduction velocities of 7 km/s and 3.9 km/s for the vertical and radial geophone components respectively to enhance visual coherency of refracted P- and S-wave arrivals. Arrival phases used in the construction of the P- and S-wave velocity models are labelled and include P-wave crustal refractions (Pg), P-wave Moho reflections (PmP), refractions converted from P- to S-waves on the way up beneath the OBS (PPS) and S-wave crustal refractions (Sg) and Moho reflections (SmS) that were converted on the way down through the crust. A converted S-wave mantle refraction (Sn, also converted on the way down) is also observable on OBS 72 (Fig. 5). Both P- and S-wave mantle refractions are observed only rarely in the region and 1D reflectivity modelling (Fuchs and Muller, 1971) indicates that this may be due to very low velocity-gradients in the upper mantle, with those phases that are observed channelled by mantle heterogeneities. Different arrival phases were identified on the basis of arrival times, move-outs and particle motions.

As secondary arrivals, the signal-to-noise ratios (SNRs) of the converted S-wave phases are inherently lower than those of the P-wave first arrivals. Standard processing steps were applied to time correct and locate the OBS (e.g., Roberts et al., 2009; White and Smith, 2009). Prior to traveltime picking of the converted phases further processing to enhance the SNR of the S-wave arrivals was also performed that included rotation of the horizontal components to transverse and radial components and application of an fk-filter to attenuate other phases (Eccles et al., 2009a).

The effect of applying these processing steps is shown in Fig. 7. The traveltimes of arrivals were picked on the first coherent peak. The polarity of the data was reversed for shots northwest of the OBSs to allow a consistent S-wave phase to be picked. At similar offsets and arrival times the horizontal geophone components have lower frequency content than the vertical component due to poor horizontal coupling (Paffenholz et al., 2005), resulting in different non-linear transfer functions for the vertical and horizontal geophone components due to rocking of the OBS. The S-wave arrivals also have lower frequencies than the P-wave equivalents due to greater frequency-dependent attenuation of the slower-propagating, shorter-wavelength phase (as shown by Fig. 2). For the S-waves the increased attenuation of the high frequencies negate any increase in spatial resolution that may have been expected from the shorter wavelength. Analysis of the particle motions of different arrivals show, as expected, markedly different behaviour for P- and S-waves (Fig. 7D and E respectively) but the linearity of such particle motions is dependent on the SNR and hence only the results from the clearest, highest amplitude phases are shown in Fig. 7. A significant amount of energy is also recorded on the transverse component (Fig. 7C); in an isotropic, homogeneous or smoothly varying medium all of the S-wave energy should be concentrated on the radial component. This energy on the transverse component may be caused by out-of-plane crustal scattering or by S-wave splitting in anisotropic regions within the crust. Some degree of S-wave splitting is indicated by phase differences between the radial and transverse components, but is difficult to quantify uniquely.

Unlike P-waves, where first arrivals are used routinely to develop tomographic velocity models (e.g., Zelt and Barton, 1998), converted

S-wave arrivals have to be considered more carefully prior to inversion for velocity structure because the interfaces at which the conversions occurred must first be determined. The sediment-top basalt boundary was found to be the primary conversion interface (Eccles et al., 2009a) with the later arrival of any conversions occurring at the seafloor obscured by the 'ringy' coda associated with the limited frequency range. The often significant traveltime delays between the PPS phases converted on the way up at the basalt-sediment interface and the pure P-wave phases (dominantly observed on the radial and vertical components respectively as shown in Fig. 7) were used to determine the Vp/Vs structure of the post-volcanic sedimentary sequence, while Sg and SmS phases, converted at sediment-top basalt interface on the way down, constrained the crustal S-wave velocities.

The SNR of the wide-angle arrivals on both Profiles 1 and 2 decreases towards the southeast. This is particularly noticeable for S-wave arrivals, which generally could not be identified on OBSs in the Faroe-Shetland Trough or Hatton Basin. This is likely to be due to the combined effect of decreased conversion efficiency and increased crustal attenuation. The post-volcanic sediment pile thickens and becomes consolidated to the southeast as the basalt thins towards the feather edge. This leads to a convergence of sediment and basalt P-wave velocities as the velocities of the more consolidated sediments increase and the bulk velocity of the basalt decreases with increasing proportions of low velocity flow margins and interbedded material. The Zoeppritz equations (Aki and Richards, 2002) indicate that such velocity trends will result in decreased mode conversion. While this explains the lack of recorded S-wave arrivals from shots in the Faroe-Shetland Trough and Hatton Basin (e.g., Fig. 6), it cannot explain the P-wave trend and asymmetry of arrivals from shots over the Fugloy Ridge and Hatton Bank. Increased P- and S-wave attenuation at the continental ends of the profiles is likely to result from the thickened sedimentary section and high impedance-contrast intrusions in the sedimentary basins and continental crust. Fault zones and fractures (Humphrey and Anderson, 1992) within the continental crust associated with multiple compressional and extensional phases of deformation (e.g., Dean et al., 1999) also contribute to the crustal attenuation. Thus, despite thinning and feathering out of the attenuative flood basalt sequences the S-wave data quality is poorest for continental crust.

## 3. Travelttime tomography

Picking errors, considerably larger for the secondary S-wave arrivals than for the P-waves, were assigned based on the arrival SNR and coherency. The picking errors associated with the PPS phases lead to uncertainty in the post-volcanic sediment Vp/Vs ratios which, as they were fixed during modelling of the crust, add to the uncertainty of the later arrivals. Initial quality control of the S-wave arrivals was carried out by comparing travelttime corrected, pseudo-reciprocal raypaths (Eccles et al., 2009a).

The layer-based parameterisation of Rayinvr (Zelt and Smith, 1992) allows a full exploration of the conversion phases and travelttime fits. During forward modelling fixed Vp/Vs ratios are specified within individual model blocks or layers, but this leads to a discontinuous S-wave velocity model even if the underlying P-wave velocity model (Roberts et al., 2009; White and Smith, 2009), determined using a least structure philosophy, is smooth. By fixing the Moho structure and the MCS determined P-wave velocities above the sediment-top basalt interface, converting P-velocities below this interface to S-velocities using a variety of constant Vp/Vs ratios and specifying conversion interfaces to give the correct path, initial smooth S-wave velocity models for Profiles 2 and 3 on the Hatton Bank margin could be developed (Eccles et al., 2009a). Inversions for S-wave velocities were then performed from the top of the igneous crust down.

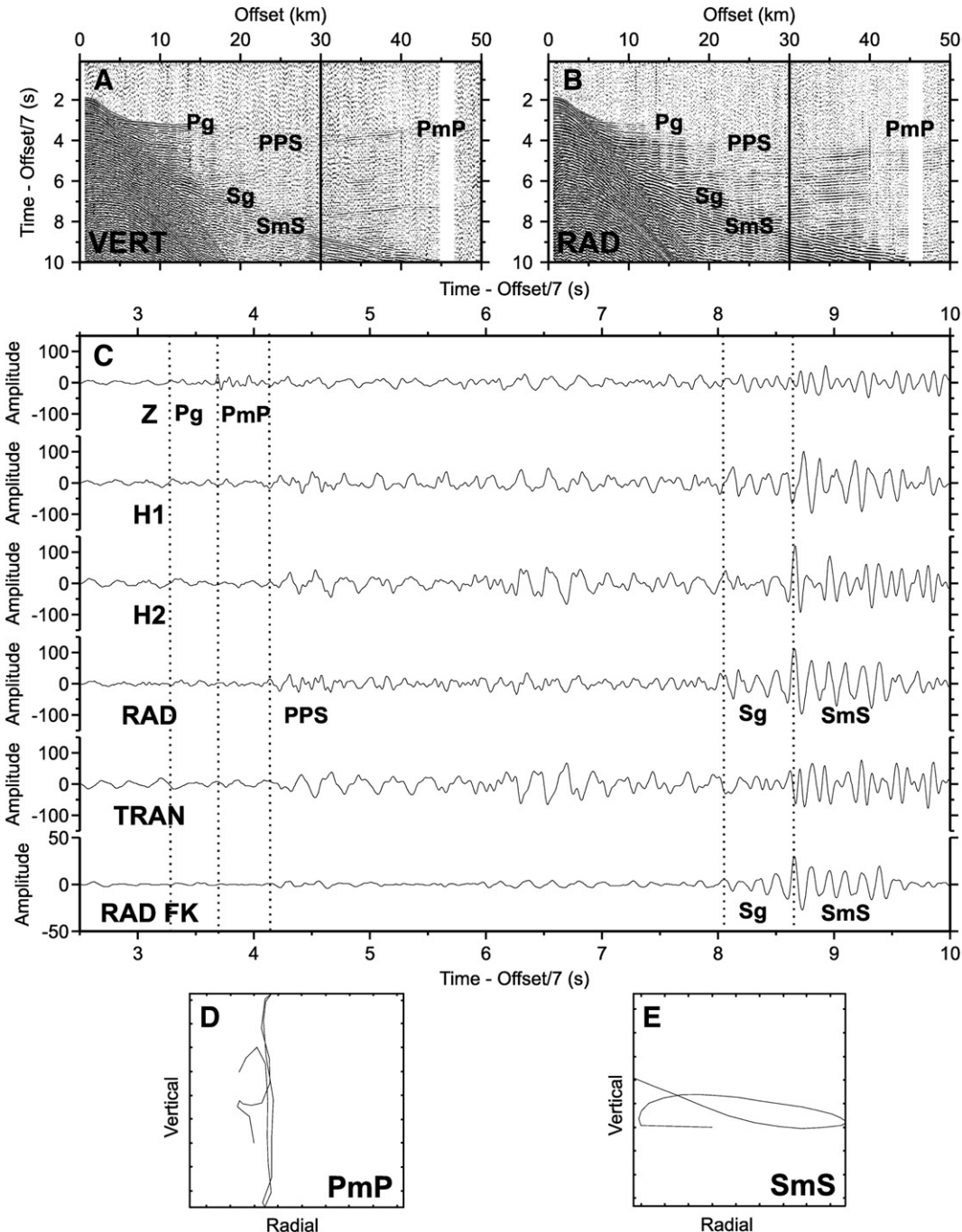


**Fig. 7.** Seismic data from OBS 73 at the oceanic end of Profile 2. A. Vertical geophone component displayed with a reduction velocity of 7 km/s. The trace shown in C at 30 km offset is highlighted. B. Radial component displayed with a reduction velocity of 7 km/s. The trace shown in C at 30 km offset is highlighted. C. The first trace (Z) is the vertical geophone component of the gimballed OBS at 30 km offset while the second and third traces (H1 and H2) represent the arbitrarily oriented horizontal geophone components. Compressional wave arrivals (e.g., Pg and PmP) are best resolved on the vertical component. The horizontal components can be rotated into radial (RAD) and transverse (TRAN) components to improve the signal-to-noise ratio of the converted shear wave arrivals, PPS, Sg and SmS. An fk-filter, in this case attenuating phases with an apparent velocity greater than 4.2 km/s, can also be applied to the radial component to reduce the interference of the P-wave energy (RAD FK) to provide better resolution of the S-wave phases converted while propagating downward. D. Particle motion of the PmP arrival for the highlighted trace. E. Particle motion of the SmS arrival for the highlighted trace.

For Profile 1 across the Faroes margin, Roberts et al. (2009) inverted for the P-wave velocities across much of the profile but forward modelled a sub-basalt P-wave low velocity zone (LVZ) to fit the observed P-wave traveltimes 'stepbacks'. They then confirmed the velocity structure by waveform modelling. Equivalent S-wave 'stepbacks', indicating that an S-wave LVZ is present, were also observed. Diving waves do not turn in LVZs and hence the LVZ velocity was unconstrained by traveltime inversion. In order to place constraints on the range of possible Vp/Vs ratios the model structure from Roberts

et al. (2009) was used and the LVZ Vp/Vs ratio was set during inversion in 0.05 increments between 1.60 and 2.10. Carrying the inversions to completion allowed an estimate of the Vp/Vs ratio of  $1.80 \pm 0.15$  to be made based on the traveltimes fits of the sub-LVZ refractions. Refining this estimate based on the relative P- and S-wave stepback times gave a Vp/Vs ratio of  $1.81 \pm 0.11$  (Eccles et al., 2009b). Rayinvr modelling also validated traveltime corrections applied to the S-wave arrivals with asymmetric raypaths to make them effective double mode-converted arrivals with both up-going and down-going

conversions at the sediment–top basalt interface. These traveltime corrections enabled the dataset to be used in inversions with a grid-based parameterisation (e.g., Tomo2D; Korenaga et al., 2000).

The regularised grid parameterisation and more automated inversion of Tomo2D (Korenaga et al., 2000) allows us to make extensive parameter testing and a less subjective inversion to be performed than when using the forward modelling program Rayinvr (Zelt and Smith, 1992). Variable damping was applied to the models during inversion to fix the velocities in the post-basalt sedimentary sequence and therefore preserve the validity of the traveltime correction. Node spacing, damping and smoothing parameters were selected to give the best trade-off between model roughness and statistical fit. Once these parameters were chosen, Monte Carlo analyses with 100 realisations were performed to explore the model spaces for the different profiles by randomising the starting models and traveltimes (Eccles et al., 2009a). A full discussion of parameter selection and randomisation processes is given by Eccles et al. (2009a). The average models, showing the structure required by the traveltimes rather than simple consistency with them, were calculated and the standard deviation, valid in areas where there was sufficient ray coverage to alter the input model distribution, gives a measure of model uncertainty. For Profile 1 across the Faroes margin this approach, although giving insight into the model uncertainty for the oceanic crust and COT, only poorly resolves the sub-basalt LVZ and hence the Rayinvr model remains the best profile-wide model. The final Profile 1 (Faroes) Rayinvr, and Profile 2 and 3 (Hatton Bank) Tomo2D, P- and S-wave velocity models are shown in Fig. 8. With the exception of the Profile 1 (Faroes) Rayinvr model (Roberts et al., 2009) the P-wave modelling was re-run in this study using the combined and amended picks of Parkin and White

(2008) and White and Smith (2009) to ensure the consistent parameterisation of the P- and S-wave models.

The spatial variation in the Vp/Vs ratio can be estimated by comparison of the P- and S-wave velocity models (Fig. 8). Although the comparison is not valid for individual model nodes, the smoothed results show the general trends. For the Tomo2D Monte Carlo results, the P- and S-wave uncertainties allow the uncertainty of the calculated Vp/Vs ratio to be determined and the images (Fig. 8H and I) are limited to regions with Vp/Vs uncertainty <0.06.

#### 4. Oceanic crust

The P-wave velocity structure of the oceanic crust is generally well resolved and the wide-angle converted S-wave arrivals allow the S-wave velocity structure to be constrained. Although the Vp/Vs structure of the post-volcanic sedimentary sequence can be determined from the comparison of the pure P-wave and the PPS phases, the S-wave velocity models of the igneous crust, and hence the determination of the Vp/Vs ratios, are less well resolved than the P-wave equivalents. This is due to the late arriving S-wave phases interfering with the water wave to offsets of up to 10–20 km (e.g., Fig. 5). The lack of short offset S-wave refractions means that the properties of oceanic layer 2 cannot be determined uniquely and the Monte Carlo analyses show high standard deviation in this area.

The properties of the oceanic lower-crust are better constrained. The P- and S-wave lower-crustal velocities modelled are higher than those expected for normal oceanic crust (White et al., 1992; Bown and White, 1994). The average lower-crustal velocity versus igneous crustal thickness

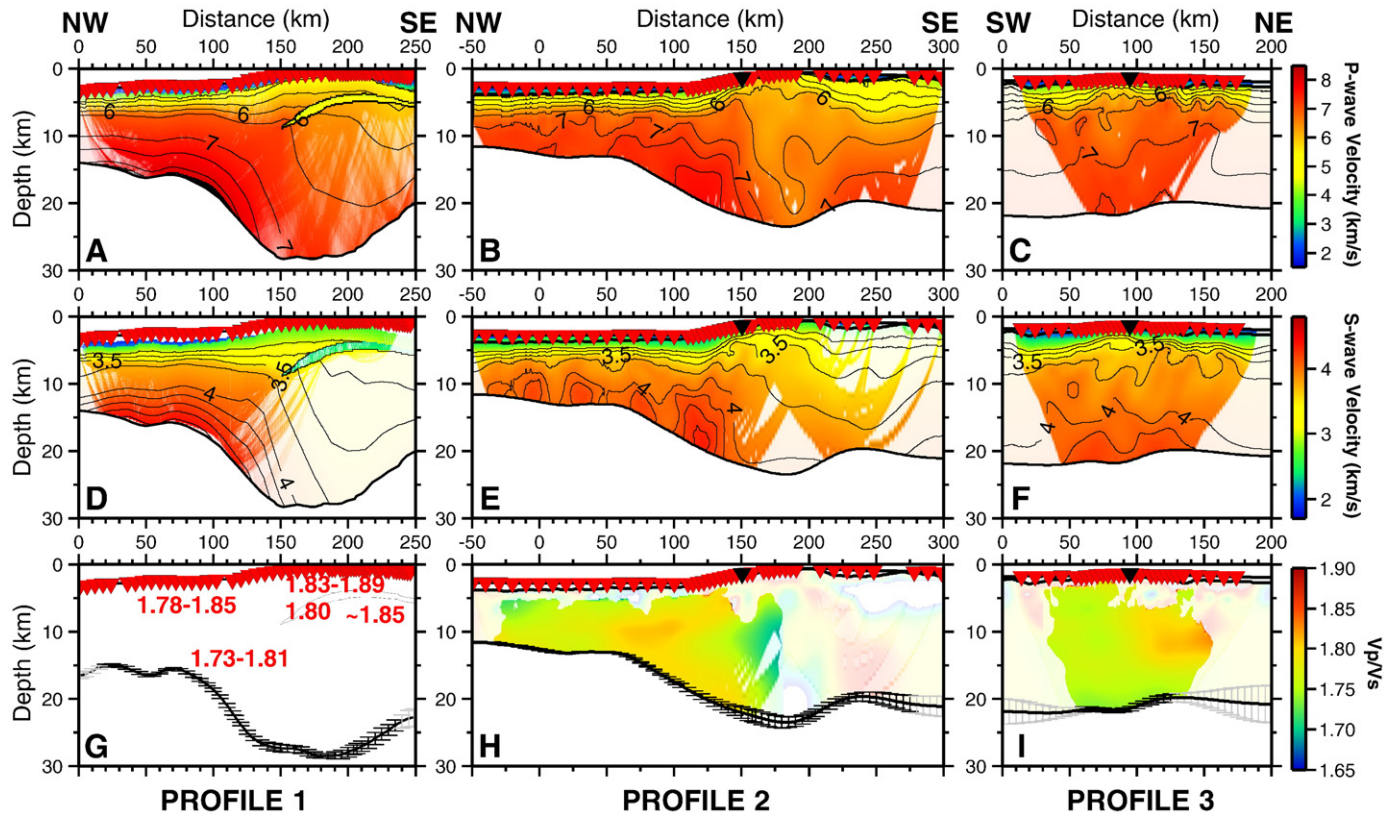


**Fig. 8.** Final results from tomographic modelling. A–C. Final P-wave velocity models for Profile 1 (Faroes), Profile 2 and Profile 3 (Hatton Bank) respectively. The Profile 1 model was produced using Rayinvr (Zelt and Smith, 1992) while Profiles 2 and 3 used Tomo2D (Korenaga et al., 2000). Contour interval 0.5 km/s except for >7 km/s where the contour interval was 0.25 km/s. D–F. Final S-wave velocity models for Profiles 1–3 respectively. The Profile 1 model was produced using Rayinvr while Profiles 2 and 3 were produced using Tomo2D. Contour interval 0.25 km/s except for velocities >4 km/s where it is 0.1 km/s. G. Vp/Vs results from the comparison of Rayinvr P- and S-wave velocity models for Profile 1. The Moho plotted, with error bars, from Monte Carlo analysis of the Tomo2D inversion is very similar to that modelled using Rayinvr. H–I. Final, smoothed Vp/Vs results for Profiles 2 and 3 respectively. Vp/Vs results have been limited to regions with uncertainty less than  $\pm 0.06$  and Gaussian smoothing (3 km vertical and 25 km horizontal) has been applied. The uncertainty in the Moho depth derived from the Monte Carlo analysis is indicated by the error bars.

trends allow discrimination between different mantle processes during oceanic crust generation (Holbrook et al., 2001; Korenaga et al., 2002). For both the Faroes and Hatton Bank margins, P- and S-wave trends across Profiles 1 and 2 indicate passive decompression of elevated-temperature mantle beneath the oceanic crust rather than active upwelling or a fertile mantle source (White et al., 2008; Eccles et al., 2009a). The high lower-crustal P-wave velocities at volcanic rifted margins have been interpreted as being caused by high magnesium concentrations (Kelemen and Holbrook, 1995). High ambient mantle temperature at the time of melt generation causes a higher magnesium melt and forsterite, magnesium-rich olivine with a P-wave velocity of ~8.6 km/s and Vp/Vs ratio of 1.71 (Christensen, 1996), is the first mineral to crystallise from the melt.

A very subtle Vp/Vs trend, smaller than the calculated uncertainty, is observed across the oceanic crust with Vp/Vs ratios decreasing by ~0.03 oceanward. This trend is inconsistent with that expected for decreasing magnesium content with decreasing ambient mantle temperature through time (as indicated by decreasing igneous crustal thickness; McKenzie and Bickle, 1988). Calculation of rock properties from the mineral composition (Hacker and Abers, 2004) suggests that the observed trend may have been caused by albite–anorthite fractionation within plagioclase feldspar (which forms up to 50% of gabbro; Le Bas and Streckeisen, 1991) or by the presence of some water within the crust that allowed increased levels of metamorphism with greater crustal thickness towards the oldest oceanic crust.

## 5. Continent–ocean transition

Trends of increasing P- and S-wave velocity and Vp/Vs ratios were observed from the continental to the oceanic crust across the COT. The average lower-crustal properties across the COT, corrected to 230 MPa and 200 °C, calculated from the Profile 1 and 2 Tomo2D inversions, are shown in Fig. 9. These results show increasing levels of mafic intrusion

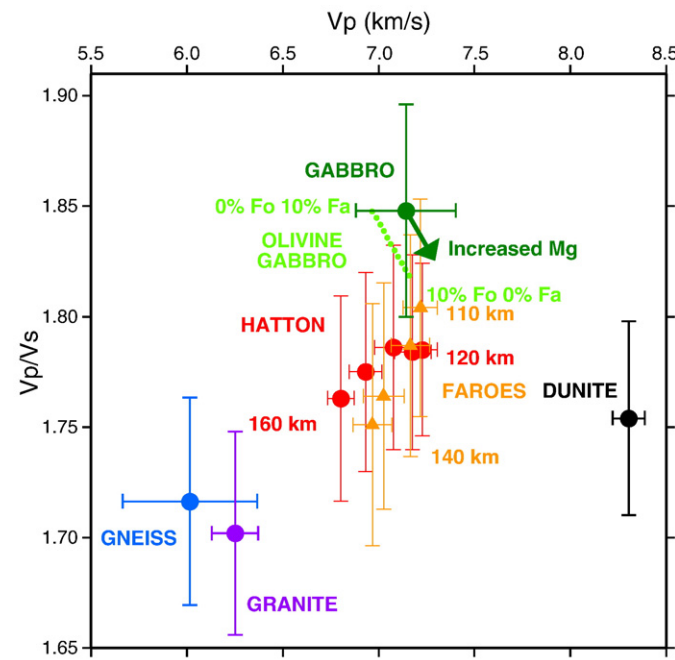


**Fig. 9.** Vp versus Vp/Vs plot of the lower-crustal properties across the COT corrected to 230 MPa and 200 °C. Profile 2 lower-crustal measurements at 10 km intervals 120–160 km are shown by red circles while the Profile 1 lower-crustal measurements at 10 km intervals 110–140 km are shown by orange triangles. The properties of dunite, gabbro, gneiss and granite (Christensen 1996) are shown by black, green, blue and purple circles respectively, corrected to 230 MPa. The properties of an Oman olive gabbro with 10% olivine (Browning, 1984) shown in pale green have been calculated (at 230 MPa and 200 °C) for systematic iron–magnesium substitution of fayalite (Fa) and forsterite (Fo) showing the Vp and Vp/Vs trend of increasing magnesium content.

into the felsic continental crust with distance across the transition (i.e., oceanward to smaller profile distances). This continental crust is likely to be Lewisian gneiss on the Faroes margin (Dean et al., 1999) and the early Proterozoic Rockall Plateau/Islay metamorphic terrane on the Hatton Bank margin (Hitchen, 2004). The mafic end of the mixing trend is not that of gabbro formed at a mid-ocean ridge but rather one, as shown by the calculated Fe–Mg trend, with a high olivine and magnesium content. That the continental crust was intruded by mafic material with contrasting physical properties, rather than being underplated by it, is indicated by prominent reflectivity in the lower-crust observed on the Profile 1 MCS image (Fig. 4). This is an important result to aid in understanding the addition of igneous rock, and the permanent uplift of marginal highs, on volcanic rifted continental margins (White et al., 2008).

A selection of P- and Vp/Vs models made across volcanic rifted continental margins in the eastern North Atlantic are shown in Fig. 10. The deployment of dense OBS arrays has become more common with time and the older models shown across the Møre and Vørting margins were constrained by comparatively few OBSs. Despite the differing approaches of inversion for least structure (this study) versus geologically layer-based inversion and forward modelling (Mjelde et al., 2003; Mjelde et al., 2008), all the profiles resolve a relatively rapid transition from a marginal high underlain by continental crust to fully oceanic crust. The profiles shown in Fig. 10A–D were produced by forward modelling Vp/Vs ratios within the layers of the P-wave velocity model while those in Fig. 10C and E were inverted for the S-wave velocity field. Forward modelling can lead to non-unique, often over-interpreted, solutions with features that, while consistent with the traveltimes dataset, may not be required by it. Hence a critical evaluation of interpretable regions and velocity and Vp/Vs values is required.

The Vp/Vs ratios of the post-volcanic sedimentary sequence are high, particularly for the youngest, least consolidated sediments, while Mesozoic sedimentary sequences are modelled to have significantly lower Vp/Vs ratios. The S-wave data quality across the continental portion of the iSMM profiles is insufficient to resolve the possible southward continuation of the high Vp/Vs lower-crust, interpreted as a mafic lower continental crust, that has been modelled on the Møre and Vørting margins (e.g., Mjelde et al., 2008) shown in Fig. 10. The crustal thickness of the marginal high is greatest at the Faroes margin, closest to the centre of magmatism, where subaerial exposure of the flood basalts are observed on the Faroe Islands (Passey and Bell, 2007).

## 6. Faroes Profile 1 LVZ and sub-LVZ

The interpretation of sub-basalt lithologies has been notoriously difficult (e.g., Archer et al., 2005) and the determination of Vp/Vs gives an additional lithology discriminator. The physical properties of the sub-basalt units determined in this study are plotted with red circles in Fig. 11. When compared with well log measurements from the Lopra-1/1A well in the Faroe Islands (Fig. 3), the P-wave velocity and Vp/Vs ratio of the LVZ are too low to be caused by a purely hyaloclastite unit, although some of this material may be present, but not separately resolvable, at the top of the LVZ or interbedded in the overlying basalt unit. The interpretation that the LVZ represents a 1–2 km thick unit of clastic sedimentary material of Early Paleocene or Mesozoic age is more likely. Although the MCS reflection image shows the region correlating to the LVZ has comparatively little reflectivity, some reflectors can be observed that may indicate the juxtaposition of shale or sand units or some sill intrusion.

Raum et al. (2005) forward modelled converted S-wave arrivals from a profile southwest of the iSMM line (Fig. 10E). The published model (Fig. 10D) indicates that some long offset, converted S-wave arrivals were recorded in this dataset to constrain the Vp/Vs ratio of the lower continental crust. The modelling of Raum et al. (2005) took a far different approach from that described in this study as constant Vp/Vs ratios were generally modelled for each layer of the P-wave

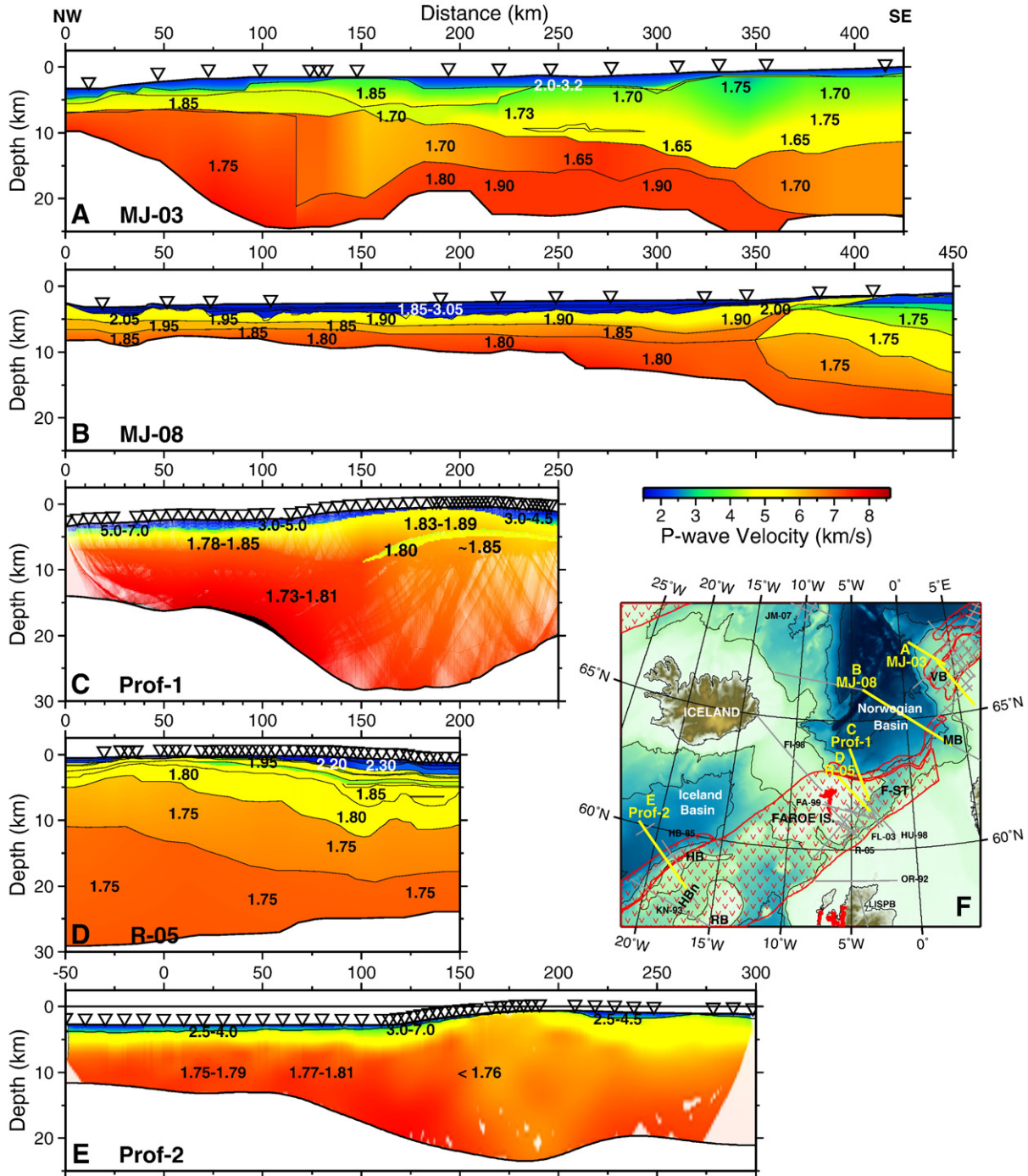


**Fig. 10.** Compilation of Vp/Vs models from along the NW European continental margin. The colour scale for A–E indicates P-wave velocity while bold numbers indicate the Vp/Vs ratio. Open triangles represent the location of OBSs. A. Profile MJ-03, a combination of profiles 1–96 and 10–96 across the Voring Margin (Mjelde et al., 2008). B. Profile MJ-08, which is Profile 1–00 across the Møre Margin (Mjelde et al., 2008). C. Oceanward subsection of iSIMM Profile 1 (Faroe margin; this study). D. Profile R-05, which is Profile 2 across the Fugloy Ridge and Faroe–Shetland Trough (Raum et al., 2005). E. Oceanward subsection of iSIMM Profile 2 (Hatton Bank; this study). F. Profile location map. The locations of the profiles shown in A–E are shown in yellow. HB = Hatton Bank, HBn = Hatton Basin, RB = Rockall Bank, F-ST = Faroe–Shetland Trough, MB = Møre Basin, VB = Voring Basin. Onshore exposures of the North Atlantic Igneous Province are shown in solid red while red patterning indicates SDRs and the extent of flood basalts. Additional wide-angle profiles, some of which were acquired with four-component OBS with potential for, or have already done, S-wave analysis, are shown in grey and include KN-93 (Keser Neish, 1993), HB-85 (Fowler et al., 1989), LISPB (Assumpcao and Bamford, 1978), OR-92 (Price and Morgan, 2000), FL-03 (Fiedner and White, 2003), HU-98 (Hughes et al., 1998), FA-99 (Richardson et al., 1999), FI-98 (Richardson et al., 1998) and JM-07 (Mjelde et al., 2007).

velocity model. The uncertainty associated with the P-wave velocity and Vp/Vs ratio of the LVZ was underestimated as the velocity-thickness ambiguity had not been discussed and the same uncertainty was assigned to the LVZ as elsewhere in the model. The results for the LVZ are comparable to those achieved in this study, although the LVZ is divided into two layers and the Vp/Vs ratios are higher than those modelled here, leading to an interpretation of Cretaceous shales. The

lower layer of the LVZ modelled by Raum et al. (2005) has properties similar to that of haloclastite (Fig. 11) but the igneous haloclastite material erupted at the beginning of the volcanic episode would be expected to overly any sedimentary deposits.

Raum et al. (2005) modelled the sub-LVZ unit, interpreted as pre-Cretaceous sedimentary rock, with a Vp/Vs ratio of 1.8, lower than that modelled (1.85) in this study. Were the LVZ to overlie the continental

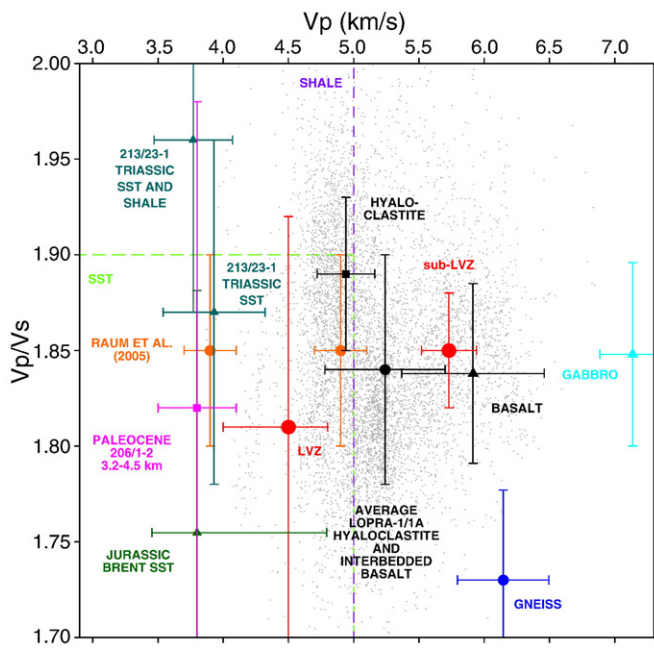


**Fig. 11.**  $V_p$  versus  $V_p/V_s$  for the LVZ and sub-LVZ resolved on Faroes Profile 1 and literature comparisons. The average results of detailed analysis of the LVZ and sub-LVZ properties from the profile-wide model are shown by the large red dots. The properties of the sub-basalt units forward modelled on a nearby profile by Raum et al. (2005) are shown by orange dots. Small grey dots represent well log measurements of hyaloclastites from the Faroe Islands Lopra-1/A well (Fig. 3); the black square is the average Lopra-1/A hyaloclastite without interbedded basalt flows, the black circle those with interbedded basalts and the black triangle an average literature value for basalt at 200 MPa (Christensen, 1996). The properties of gabbro and gneiss (Christensen, 1996), also at 200 MPa, are shown as a pale blue triangle and dark blue circle respectively. Fields defining clean sandstone and shale are shown in green and purple respectively (Tatham, 1982; Tatham and McCormack, 1991). The properties of the Paleocene sedimentary section, with  $V_s$  calculated using the mudrock relation of Castagna et al. (1985), from the deeper subsection of the 206/1-2 well (Fig. 3) are shown in pink. Examples of Mesozoic sedimentary units from the region for which S-wave sonic logs were recorded are shown by green triangles for Jurassic Brent sandstone (Strandenes, 1991) and Triassic sandstone and shale units from well 213/23-1 (courtesy of ExxonMobil).

basement directly,  $V_p/V_s$  ratios of  $\sim 1.74$  would be expected (Christensen, 1996). High  $V_p/V_s$  ratios have been measured for weathered Lewisian rocks exposed in Scotland (Hall and Simmons, 1979) but these are associated with hydration of more mafic units within the terrane with correspondingly high P-wave velocities. Although slower than expected for crystalline rock, the P-wave velocities of 5.45–5.8 km/s modelled by Raum et al. (2005) and in this study are still higher than would be expected for sedimentary rock, indicating that igneous intrusion may be pervasive within this unit. The  $V_p/V_s$  ratios can be used to estimate the quartz content and hence the sand to shale ratio. While Raum et al. (2005) estimated that the sub-LVZ unit had a higher proportion of sand than the LVZ, the study reported here indicates the reverse.

The traveltome tomography reveals a relatively thin, laterally extensive LVZ that feathers out at the COT and the physical properties of this unit have been interpreted as a sedimentary, possibly sill-intruded, unit. The sub-LVZ unit, the deepest resolved by this study, is also interpreted to be sedimentary in origin. This implies that prior to break-up there was a pre-existing sedimentary basin across what is now the Fugloy Ridge, this structural inversion due to intrusion-related uplift and Cenozoic compression (Andersen et al., 2000; Sørensen, 2003). This basin may represent the western flank of the Mesozoic Faroe–Shetland Trough.

Cretaceous and younger sedimentary sequences and basaltic units of the Kangerlussuaq Basin, East Greenland, correlate well with those of the Faroe–Shetland Trough and Faroe Islands that would have been  $<100$  km away prior to break-up (Larsen et al., 2006). The Cretaceous saw wide-scale subsidence and shale deposition in the Faroes and

Hatton Bank regions, with many of the paleohighs drowned at this time (Ziska and Andersen, 2005), and deposition in the Kangerlussuaq Basin initiated (Larsen et al., 2006). There is some palynoflora and heavy mineral evidence in the centre of the Faroe–Shetland Trough, which has remained a deep water depocentre since the Mesozoic, that sediment derived from Greenland was transported westward during the Paleocene (Jolley et al., 2005). At this time the Greenland margin underwent significant transitory uplift caused by the mantle hotspot as illustrated by fluvial deposits formed in the Kangerlussuaq Basin (Larsen et al., 2006). Weathering or remobilisation of older sediment from the continental block beneath the Faroe Islands may have also occurred during the Paleocene (Ziska and Andersen, 2005).

Thus the LVZ and sub-LVZ units modelled are interpreted as Paleocene Greenland or Faroes Platform derived sand/shale units and sill-intruded Cretaceous shales. The argument for a westerly provenance, which would allow the presence of coarser, sand-rich units than could have been derived solely from the NW European margin, is strengthened by the continuation of sub-basalt sedimentary units to the COT and has important implications for sub-basalt hydrocarbon prospecting.

## 7. Conclusions

Traveltome tomography of wide-angle arrivals recorded on four-component OBSs yields valuable information on the structure and composition of volcanic rifted continental margins in the North Atlantic. Studying the oceanic crust produced at the two margins allows the spatial and temporal changes in physical properties and igneous crustal thickness to be characterised. Passive decompression melting of elevated-temperature mantle caused a higher than normal melt fraction and the more refractory components of the melt such as iron and magnesium were crystallised in the lower-crust. The increased igneous crustal thickness and lower-crustal velocities modelled at the Faroes margin indicate that this was proximal to the hotspot, now present beneath Iceland, at the time of break-up. Subtle  $V_p/V_s$  variations across the oceanic crust, which are observed on both margins, if real, hint at fractional crystallisation or hydration processes that are not yet fully understood.

Across the COT the physical properties modelled clearly suggest the mixing of felsic continental crust and magnesium-rich mafic intrusions. This corroborates the interpretation of lower-crustal reflectivity at the COT, observed for the first time on the (Faroes) Profile 1 MCS reflection image, as an interference pattern caused by the high impedance-contrast igneous intrusions into the pre-existing continental crust. The rapid lateral variation of P-wave velocity and  $V_p/V_s$  ratios across these, and other, North Atlantic volcanic rifted continental margins suggests that extensive intrusion weakened the crust, enabling more ductile continental breakup and a much narrower COT than observed at non-volcanic margins.

The  $V_p/V_s$  ratio modelled on Profile 1 (Faroes) for units beneath the flood basalts provides additional constraint on the sub-basalt lithology and indicates that a pre-break-up (Mesozoic to possibly Paleocene) sedimentary system continued west of the well defined Faroe–Shetland Trough. This sedimentary system may have been connected to the Greenland margin which was in close proximity to this area prior to opening of the North Atlantic.

## Acknowledgements

The iSIMM Scientific Team comprises N.J. Kusznir, R.S. White, A.M. Roberts, P.A.F. Christie, R. Spitzer, N. Hurst, Z.C. Lunnon, C.J. Parkin, A.W. Roberts, L.K. Smith, V. Tymms, J.D. Eccles, R. Fletcher, A. Chappell, D. Healy, O. Lewis and H. Lau. The iSIMM project was supported by Liverpool and Cambridge Universities, Schlumberger Cambridge Research, Badley Geoscience Limited, WesternGeco, Amerada Hess, Anadarko, BP, ConocoPhillips, ENI UK, Statoil, Shell, the Natural Environment Research Council and the Department of Trade and Industry. However, the views

expressed here are those of the authors who are solely responsible for any errors. Additional thanks to ExxonMobil and IHS for allowing the publication of well results. Figures have been produced using GMT (Wessel and Smith, 1998). Department of Earth Sciences, Cambridge contribution number ES.1231.

## References

- Aki, K., Richards, P.G., 2002. Quantitative Seismology 2nd edn. University Science Books, Sausalito, CA.
- Andersen, M.S., Nielsen, T., Sorensen, A.B., Boldreel, L.O., Kuipers, A., 2000. Cenozoic sediment distribution and tectonic movements in the Faroe region. *Global and Planetary Change* 24, 239–259.
- Archer, S.G., Bergman, S.C., Iliffe, J., Murphy, C.M., Thornton, M., 2005. Paleogene igneous rocks reveal new insights into the geodynamic evolution and petroleum potential of the Rockall Trough, UK Atlantic margin. *Basin Research* 17, 171–201.
- Assumpcao, M., Bamford, D., 1978. LISPB-V. Studies of crustal shear waves. *Geophysical Journal of the Royal Astronomical Society* 54, 61–73.
- Brown, J.W., White, R.S., 1994. Variation with spreading rate of oceanic crustal thickness and geochemistry. *Earth and Planetary Science Letters* 121, 435–449.
- Browning, P., 1984. Cryptic variation within the cumulate sequence of the Oman ophiolite: magma chamber depth and petrological implications. In: Gass, I.G., Lippard, S.J., Shelton, A.W. (Eds.), Ophiolites and oceanic lithosphere. Geological Society Special Publication. The Geological Society, London, pp. 71–82.
- Castagna, J.P., Batzle, M.L., Eastwood, R.L., 1985. Relationships between compressional-wave and shear-wave velocities in clastic silicate rocks. *Geophysics* 50 (4), 571–581.
- Christensen, N.I., 1996. Poisson's ratio and crustal seismology. *Journal of Geophysical Research* 101 (B2), 3129–3156.
- Christie, P., Langridge, A., White, R., Lunnon, Z., Roberts, A.W., the iSMM team, 2004. ISIMM looks beneath basalt for both industry and university research. Proceedings of the 5th Conference and Exposition of Petroleum Geophysics, Hyderabad, India 15–17 January 2004.
- Christie, P., Gollifer, I., Cowper, D., 2006. Borehole seismic studies of a volcanic succession from the Lopra-11A borehole in the Faroe Islands, NE Atlantic. *Geology of Denmark Survey* 9, 23–40.
- Clift, P.D., 1999. The thermal impact of Paleocene magmatic underplating in the Faroe-Shetland-Rockall region. *Petroleum Geology of Northwest Europe: Proceedings of the 5th Conference*. The Geological Society, London, pp. 585–593.
- Coffin, M.F., Eldholm, O., 1994. Large igneous provinces: crustal structure, dimensions, and external consequences. *Reviews of Geophysics* 32 (1), 1–36.
- Dean, K., McLachlan, K., Chambers, A., 1999. Rifting and the development of the Faeroe-Shetland Basin. *Petroleum Geology of Northwest Europe: Proceedings of the 5th Conference*. The Geological Society, London, pp. 531–544.
- Eccles, J.D., White, R.S., Christie, P.A.F., Roberts, A.W., the iSMM team, 2009a. Identification and inversion of converted shear waves: case studies from the North Atlantic continental margins. *Geophysical Journal International* 197 (1), 381–400.
- Eccles, J.D., White, R.S., Christie, P.A.F., Roberts, A.W., the iSMM team, 2009b. Insight into sub-basalt lithology from wide-angle converted shear wave analysis. *Faroe Islands Exploration Conference: Proceedings of the 2nd Conference*, vol. 48 of *Annales Societatis Scientiarum Faeroensis*, Tórshavn, pp. 35–52.
- Eldholm, O., Grue, K., 1994. North Atlantic volcanic margins: dimensions and production rates. *Journal of Geophysical Research* 99 (B2), 2955–2968.
- Fiedler, M.M., White, R.S., 2003. Depth imaging of basalt flows in the Faeroe–Shetland Basin. *Geophysical Journal International* 152 (2), 353–371.
- Foulger, G.R., Natland, J.H., Anderson, D.L., 2005. Genesis of the Iceland Melt anomaly by plate tectonic processes. In: Foulger, G.R., Natland, J.H., Presnall, D.C., Anderson, D.L. (Eds.), Plates, Plumes and Paradigms, vol. 388 of Special Paper, The Geological Society of America. The Geological Society of America, pp. 595–625.
- Fowler, S.R., White, R.S., Spence, G.D., Westbrook, G.K., 1989. The Hatton Bank continental margin – II. Deep structure from two-ship expanding spread seismic profiles. *Geophysical Journal* 96, 295–309.
- Fuchs, K., Muller, G., 1971. Computation of synthetic seismograms with the reflectivity method and comparison with observations. *Geophysical Journal of the Royal Astronomical Society* 23, 417–433.
- Glennie, K.W., 1995. Permian and Triassic rifting in northwest Europe. In: Boldy, S.A.R. (Ed.), Permian and Triassic Rifting in Northwest Europe, vol. 91 of Geological Society Special Publication. The Geological Society, London, pp. 1–5.
- Hacker, B.R., Abers, G.A., 2004. Subduction Factory 3: an Excel worksheet and macro for calculating densities, seismic wave speeds, and H<sub>2</sub>O contents of minerals and rocks at pressure and temperature. *Geochemistry Geophysics Geosystems* 5 (1), Q01005.
- Hall, J., Simmons, G., 1979. Seismic velocities of Lewisian metamorphic rocks at pressures to 8 kbar: relationship to crustal layering in North Britain. *Geophysical Journal of the Royal Astronomical Society* 58, 337–347.
- Hitchen, K., 2004. The geology of the UK Hatton–Rockall margin. *Marine and Petroleum Geology* 21, 993–1012.
- Holbrook, W.S., Larsen, H.C., Korenaga, J., Dahl-Jensen, T., Reid, I.D., Kelemen, P.B., Hoppe, J.R., Kent, G.M., Lizarralde, D., Bernstein, S., Detrick, R.S., 2001. Mantle thermal structure and active upwelling during continental breakup in the North Atlantic. *Earth and Planetary Science Letters* 190, 251–266.
- Hughes, S., Barton, P.J., Harrison, D., 1998. Exploration in the Shetland–Faeroe basin using densely spaced arrays of ocean-bottom seismometers. *Geophysics* 63 (2), 490–501.
- Humphrey, J.R., Anderson, J.G., 1992. Shear-wave attenuation and site response in Guerrero, Mexico. *Bulletin of the Seismological Society of America* 81 (4), 1622–1645.
- Jolley, D.W., Morton, A., Prince, I., 2005. Volcanogenic impact on phytogeography and sediment dispersal patterns in the NE Atlantic. *Petroleum Geology: North-West Europe and Global Perspectives – Proceedings of the 6th Petroleum Geology Conference*. The Geological Society, London, pp. 969–975.
- Kelemen, P.B., Holbrook, W.S., 1995. Origin of thick high velocity igneous crust along the U.S. East Coast Margin. *Journal of Geophysical Research* 100 (B7), 10077–10094.
- Keser Neish, J., 1993. Seismic structure of the Hatton–Rockall area: an integrated seismic/modelling study from composite datasets. *Petroleum Geology f Northwest Europe: Proceedings of the 4th Conference*. The Geological Society, London, pp. 1047–1056.
- Korenaga, J., Holbrook, W.S., Kent, G.M., Kelemen, P.B., Detrick, R.S., Larsen, H.C., Hoppe, J.R., Dahl-Jensen, T., 2000. Crustal structure of the southeast Greenland margin from joint refraction and reflection seismic tomography. *Journal of Geophysical Research* 105 (B9), 21591–21614.
- Korenaga, J., Kelemen, P.B., Holbrook, W.S., 2002. Methods for resolving the origin of large igneous provinces from crustal seismology. *Journal of Geophysical Research* 107 (B9), 2178.
- Larsen, M., Knudsen, C., Frei, D., Frei, M., Rasmussen, T., Whitham, A.G., 2006. East Greenland and Faroe–Shetland sediment provenance and Palaeogene sand dispersal systems. *Geological Survey of Denmark and Greenland Bulletin* 10, 29–32.
- Lay, T., Wallace, T.C., 1995. Modern Global Seismology. Academic Press, USA.
- Le Bas, M.J., Streckeisen, A.L., 1991. The IUGS systematics of igneous rocks. *Journal of the Geological Society of London* 148, 825–833.
- Lunnon, Z.C., Christie, P.A.F., White, R.S., 2003. An evaluation of peak and bubble tuning in sub-basalt seismology: modelling and results from OBS data. *First Break* 21, 51–56.
- Maresh, J., White, R.S., 2005. Seeing through a glass, darkly: strategies for imaging through basalt. *First Break* 23, 27–33.
- Maresh, J., White, R.S., Hobbs, R.W., Smallwood, J.R., 2006. Seismic attenuation of Atlantic margin basalts: observations and modeling. *Geophysics* 71 (6), 211–221.
- McKenzie, D., Bickle, M.J., 1988. The volume and composition of melt generated by extension of the lithosphere. *Journal of Petrology* 29, 625–679.
- Menzies, M.A., Klemperer, S.L., Ebinger, C.J., Baker, J., 2002. Characteristics of volcanic rifted margins. In: Menzies, M.A., Klemperer, S.L., Ebinger, C.J., Baker, J. (Eds.), volcanic rifted margins, vol. 362. Geological Society of America, pp. 1–14.
- Mjelde, R., Raum, T., Digranes, P., Shimamura, H., Shiobara, H., Kodaira, S., 2003. Vp/Vs ratio along the Voring Margin, NE Atlantic, derived from OBS data: implications on lithology and stress field. *Tectonophysics* 369, 175–197.
- Mjelde, R., Eckhoff, I., Solbakken, S., Kodaira, S., Shimamura, H., Gunnarsson, K., Nakanishi, A., Shiobara, H., 2007. Gravity and S-wave modelling across the Jan Mayen Ridge, North Atlantic: implications for crustal lithology. *Marine Geophysical Research* 28, 27–41.
- Mjelde, R., Raum, T., Breivik, A.J., Faleide, J.I., 2008. Crustal transect across the North Atlantic. *Marine Geophysical Researches* 29, 73–87.
- Mutter, J.C., Talwani, M., Stoffa, P.L., 1982. Origin of seaward dipping reflectors in oceanic crust off the Norwegian margin by "subaerial seafloor spreading". *Geology* 10, 353–357.
- Nakamura, Y., Koyama, J., 1982. Seismic Q of the lunar upper mantle. *Journal of Geophysical Research* 87 (B6), 4855–4861.
- Newman, R., White, N., 1997. Rheology of the continental lithosphere inferred from sedimentary basins. *Nature* 385, 621–624.
- Paffenholz, J., Shurtliff, R., Hays, D., Docherty, P., 2005. Evolution of a multicomponent autonomous OBS: the role of geophysics. EAGE/SEG Research Workshop 'Multicomponent Seismic – Past, Present and Future' Extended Abstracts, A12.
- Parkin, C.J., White, R.S., 2008. Influence of the Iceland mantle plume on oceanic crust generation in the North Atlantic. *Geophysical Journal International* 173 (1), 168–188.
- Passe, S.R., Bell, B.R., 2007. Morphologies and emplacement mechanisms of the lava flows of the Faroe Island Basalt Group, Faroe Islands, NE Atlantic Ocean. *Bulletin of Volcanology* 70 (2), 139–156.
- Planke, S., Eldholm, O., 1994. Seismic response and construction of seaward dipping wedges of flood basalts: Voring volcanic margin. *Journal of Geophysical Research* 99 (B5), 9263–9278.
- Planke, S., Alvestad, E., Eldholm, O., 1999. Seismic characteristics of basalt extrusive and intrusive rocks. *The Leading Edge* 18 (3), 342–348.
- Price, C., Morgan, J., 2000. Lithospheric structure north of Scotland – II. Poisson's ratios and waveform modelling. *Geophysical Journal International* 142, 737–754.
- Pujol, J., Smithson, S., 1991. Seismic wave attenuation in volcanic rocks from VSP experiments. *Geophysics* 56 (9), 1441–1455.
- Raum, T., Mjelde, R., Berge, A.M., Paulsen, J.T., Digranes, P., Shimamura, H., Shiobara, H., Kodaira, S., Larsen, V.B., Fredsted, R., Harrison, D.J., Johnson, M., 2005. Sub-basalt structures east of the Faroe Islands revealed from wide-angle seismic and gravity data. *Petroleum Geoscience* 11, 291–308.
- Richardson, K.R., Smallwood, J.R., White, R.S., Snyder, D.B., Maguire, P.K.H., 1998. Crustal structure beneath the Faroe Islands and the Faroe–Iceland Ridge. *Tectonophysics* 300, 159–180.
- Richardson, K.R., White, R.S., England, R.W., Fruehn, J., 1999. Crustal structure east of the Faroe Islands: mapping sub-basalt sediments using wide-angle seismic data. *Petroleum Geoscience* 5, 161–172.
- Roberts, A.W., White, R.S., Christie, P.A.F., 2009. Imaging igneous rocks on the North Atlantic rifted continental margin. *Geophysical Journal International* 179 (2), 1024–1038.
- Rutledge, J.T., Winkler, H., 1989. Attenuation measurements from vertical seismic profile data: Leg 104, Site 642. In: Eldholm, O., Thiede, E. (Eds.), *Proceedings of the Ocean Drilling Program: Scientific Results*, vol. 104. National Science Foundation, pp. 965–972.
- Scheirer, D.S., Hobbs, R.W., 1990. Seismic attenuation in the continental crust SW of England. *Geophysical Journal International* 103, 533–540.

- Self, S., Blake, S., Sharma, K., Widdowson, M., Sephton, S., 2008. Sulfur and chlorine in Late Cretaceous Deccan magmas and eruptive gas release. *Science* 319, 1654–1657.
- Shaw, F., Worthington, M.H., White, R.S., Andersen, M.S., Petersen, U.K., Seifab Group, 2008. Seismic attenuation in Faroe Island basalts. *Geophysical Prospecting* 56 (1), 5–20.
- Sheth, H.C., 1999. Flood basalts and large igneous provinces from deep mantle plumes: fact, fiction, and fallacy. *Tectonophysics* 311, 1–29.
- Smallwood, J.R., White, R.S., 2002. Ridge–plume interaction in the North Atlantic and its influence on continental breakup and seafloor spreading. In: Jolley, D.W., Bell, B.R. (Eds.), *The North Atlantic Igneous Province: Stratigraphy, Tectonic, Volcanic and Magmatic Processes*, vol. 197 of Geological Society Special Publication. The Geological Society, London, pp. 15–37.
- Sørensen, A.B., 2003. Cenozoic basin development and stratigraphy of the Faroes area. *Petroleum Geoscience* 9, 189–207.
- Spence, G.D., White, R.S., Westbrook, G.K., Fowler, S.R., 1989. The Hatton Bank continental margin – I. Shallow structure from two-ship expanding spread seismic profiles. *Geophysical Journal* 96, 273–294.
- Spitzer, R., White, R.S., Christie, P.A.F., the iSIMM Team, 2008. Seismic characterization of basalt flows from the Faroes margin and Faroe–Shetland basin. *Geophysical Prospecting* 56, 21–31.
- Strandenes, S., 1991. Rock physics analysis of the Brent Group reservoir in the Oseberg Field. Stanford Rockphysics and Borehole Geophysics Project, Special Volume, Stanford University.
- Tatham, R.H., 1982. Vp/Vs and lithology. *Geophysics* 47 (3), 336–344.
- Tatham, R.H., McCormack, M.D., 1991. Rock physics measurements. *Multicomponent Seismology in Petroleum Exploration*. Society of Exploration Geophysicists, pp. 43–89.
- Wessel, P., Smith, W.H.F., 1998. New, improved version of Generic Mapping Tools released. *EOS, Transactions, American Geophysical Union* 79 (47), 579.
- WesternGeco, 2002. Q-marine seismic acquisition results: reports from WesternGeco. First Break 20, 778–781.
- White, R.S., Smith, L.K., 2009. Crustal structure of the Hatton volcanic rifted continental margin, NE Atlantic and mantle thermal anomalies. *Journal of Geophysical Research* 114, B02305. doi:10.1029/2008JB005856.
- White, R.S., McKenzie, D., O’Nions, R.K., 1992. Oceanic crustal thickness from seismic measurements and rare earth element inversion. *Journal of Geophysical Research* 97 (B13), 19683–19715.
- White, R.S., Smallwood, J.R., Fliedner, M.M., Boslaugh, B., Maresh, J., Fruehn, J., 2003. Imaging and regional distribution of basalt flows in the Faroe–Shetland Basin. *Geophysical Prospecting* 51, 215–231.
- White, R.S., Smith, L.K., Roberts, A.W., Christie, P.A.F., Kusznir, N.J., iSIMM Team, 2008. Lower-crustal intrusion on the North Atlantic continental margin. *Nature* 452, 460–465.
- Zelt, C.A., Barton, P.J., 1998. Three-dimensional seismic refraction tomography: a comparison of two methods applied to data from the Faeroe Basin. *Journal of Geophysical Research* 103 (B4), 7187–7210.
- Zelt, C.A., Smith, R.B., 1992. Seismic travel time inversion for 2-D crustal velocity structure. *Geophysical Journal International* 108, 16–34.
- Ziska, H., Andersen, C., 2005. Exploration opportunities in the Faroe Islands. Faroe Islands Exploration Conference: Proceedings of the 1st Conference, vol.43 of *Annales Societatis Scientiarum Faeroensis*, Tórshavn, pp. 146–162.